

# Shear wave induced resonance elastography of spherical masses with polarized torsional waves

Anis Hadj Henni,<sup>1</sup> Cédric Schmitt,<sup>1,2</sup> Isabelle Trop,<sup>3,4</sup> and Guy Cloutier<sup>1,2,4,a)</sup>

<sup>1</sup>Laboratory of Biorheology and Medical Ultrasonics, University of Montreal Hospital Research Center (CRCHUM), Montreal, Quebec H2L 2W5, Canada

<sup>2</sup>Institute of Biomedical Engineering, University of Montreal, Montreal, Quebec H3C 3J7, Canada

<sup>3</sup>Department of Radiology, University of Montreal Hospital (CHUM), Montreal, Quebec H2L 4M1, Canada

<sup>4</sup>Department of Radiology, Radio-Oncology and Nuclear Medicine, University of Montreal, Montreal, Quebec H3T 1J4, Canada

(Received 26 August 2011; accepted 29 February 2012; published online 26 March 2012)

Shear wave induced resonance (SWIR) is a technique for dynamic ultrasound elastography of confined mechanical inclusions. It was developed for breast tumor imaging and tissue characterization. This method relies on the polarization of torsional shear waves modeled with the Helmholtz equation in spherical coordinates. To validate modeling, an *in vitro* set-up was used to measure and image the first three eigenfrequencies and eigenmodes of a soft sphere. A preliminary *in vivo* SWIR measurement on a breast fibroadenoma is also reported. Results revealed the potential of SWIR elastography to detect and mechanically characterize breast lesions for early cancer detection. © 2012 American Institute of Physics. [<http://dx.doi.org/10.1063/1.3696300>]

Ultrasound (US) B-mode imaging is a standard radiological diagnostic modality to detect abnormal breast masses. However, additional quantitative assessment would likely enhance current accuracy of US. For this purpose, dynamic elastography (DE) was introduced to quantify mechanical properties of breast tissues.<sup>1,2</sup> As a complementary DE modality, we recently proposed the shear wave induced resonance elastography (SWIRE) technique. It relies on shear resonance properties of confined mechanical heterogeneities.<sup>3</sup> The technique consists to adapt the polarization of shear waves to the geometry of the heterogeneous mass, perform a frequency scan to identify its eigenfrequencies, and image corresponding eigenmodes. At resonance, SWIRE enhances the identification of a mechanically soft mass embedded in a harder medium. Results are demonstrated for inclusions larger than 5 mm (16 mm diameter *in vitro* and 11 mm by 5 mm *in vivo*). This study introduces the theoretical and experimental validation of SWIRE for the imaging and characterization of spherical masses.

Torsional shear waves were coupled to SWIRE. To model this elastodynamic problem, a perfectly spherical heterogeneity diffracting an incident torsional wave was postulated. In addition, the wave rotational axis was assumed to coincide with one symmetry axis of the sphere. Under these conditions, when a torsional incident shear wave is scattered by a spherical inclusion of radius  $R$ , embedded in a mechanically different material, it does not produce mode conversions and both diffracted and refracted elastic waves are purely circumferential. Let assume a plane torsional incident wave polarized, in a spherical system of coordinates ( $\theta$ ,  $\mathbf{e}_r$ ,  $\mathbf{e}_\theta$ ,  $\mathbf{e}_\varphi$ ), in the circumferential direction and propagating following the  $z$  axis, as represented in Figure 1. The materials of the sphere (medium 1) and that of the surrounding tissue (medium 2) are assumed homogeneous, isotropic, and linear

viscoelastic. Displacements have one non-zero component following the circumferential unit vector  $\mathbf{e}_\varphi$  and depend on the radial ( $r$ ) and angular ( $\theta$ ) coordinates. In this case, the Navier differential equation, which governs the displacement field in both media,<sup>4</sup> is simplified to the classical Helmholtz equation. In the frequency domain, assuming an implicit harmonic dependence  $e^{i\omega t}$ , this is expressed as

$$\mu_j(\Delta \mathbf{U}_j) + \rho_j \omega^2 \mathbf{U}_j = 0, \quad (1)$$

where  $j = \{1, 2\}$  designates the medium,  $\mathbf{U}_j = U_j(r, \theta) \mathbf{e}_\varphi$  is the stationary displacement field in the medium  $j$ , whereas  $\omega$ ,  $\rho_j$ , and  $\mu_j$  are the wave angular frequency, density, and complex viscoelastic shear modulus of the considered medium, respectively.

In the following, the wave number in each medium is defined by  $k_{Tj} = \omega / c_{Tj}$ , where  $c_{Tj}$  is the torsional shear wave velocity. In a spherical system of coordinates, an incident plane torsional (circumferential) shear wave can be expressed as<sup>5</sup>

$$U(r, \theta)_{inc} = \sum_{n=1}^{+\infty} Amp(\omega) i^n \frac{2n+1}{n(n+1)} \times j_n(k_{T2} r) \frac{\partial}{\partial \theta} [P_n^m(\cos \theta)] \cos m\varphi, \quad (2)$$

where  $Amp(\omega)$  is the incident wave amplitude,  $j_n(\cdot)$  is the first kind spherical Bessel function, and  $P_n^m(\cdot)$  is the associated Legendre function. Since the displacement field does not depend on the angle  $\varphi$ , the  $m$  index equals zero. This allows simplifying the incident shear wave expression. In the same way, the scattered and refracted displacement fields are solutions of Eq. (1), which can be solved in a spherical system of coordinates by mean of spherical Bessel functions and associated Legendre functions product series.<sup>5,6</sup>

In the surrounding medium 2, the resulting displacement field is a combination of the known incident plane wave and

<sup>a)</sup>Author to whom correspondence should be addressed. Electronic mail: [guy.cloutier@umontreal.ca](mailto:guy.cloutier@umontreal.ca). Tel.: +1 514-890-8000 (24703). Fax: +1 514-412-7505.

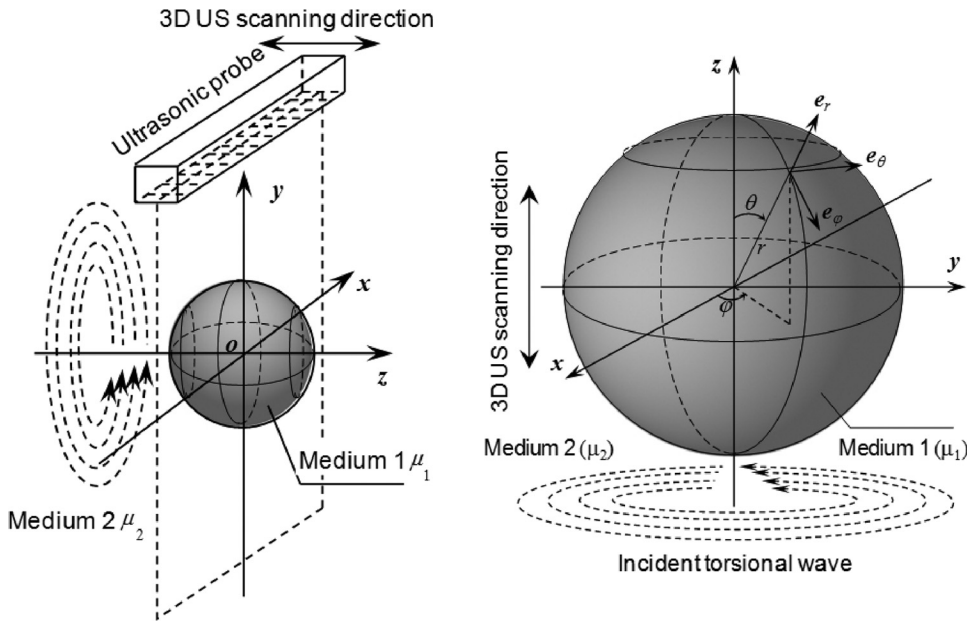


FIG. 1. Left: Representation of the experimental configuration used to measure resonance spectra and to image the spherical heterogeneity eigenmodes. Right: 3D representation of torsional waves scattering by a spherical heterogeneity embedded in a homogeneous medium. A spherical system of coordinates was used for the modeling.

the scattered one. This latter and the refracted torsional wave can be expressed using series containing unknown coefficients  $A_n$  and  $B_n$ , as follows:

$$\begin{aligned}
 U(r, \theta)_1 &= \sum_{n=1}^{+\infty} A_n j_n(k_{T_1} r) P_n^1(\cos \theta) \\
 U(r, \theta)_2 &= \sum_{n=1}^{+\infty} (Amp(\omega) i^n \frac{2n+1}{n(n+1)} j_n(k_{T_2} r) \\
 &\quad + B_n h_n^{(1)}(k_{T_2} r)) P_n^1(\cos \theta), \quad (3)
 \end{aligned}$$

where  $h_n^{(1)}(\cdot)$  is the first kind spherical Hankel function. Coefficients  $A_n$  and  $B_n$  are calculated by taking into account the continuity of displacements  $U_1$  and  $U_2$ , and normal stresses  $\sigma_1$  and  $\sigma_2$  at the boundary of the spherical heterogeneity

$$\begin{cases} U_1(r=R, \theta) = U_2(r=R, \theta) \\ \sigma_{r\varphi_1}(r=R, \theta) = \sigma_{r\varphi_2}(r=R, \theta) \end{cases} \quad \text{with } \theta \in [0, \pi] \quad (4)$$

Using displacements of Eq. (3) and expressing the normal stress at  $r=R$ , one obtains a system of two equations containing the infinite set of unknowns. The orthogonality property of associated Legendre functions permits to separate

Eq. (4) into an infinite set of linear equations with respect to the integer order  $n$

$$\mathbf{T}_n \begin{pmatrix} A_n \\ B_n \end{pmatrix} = \mathbf{b}_n, \quad r=R \quad \text{and} \quad n=0, \dots, +\infty. \quad (5)$$

In Eq. (5),  $\mathbf{T}_n$  and  $\mathbf{b}_n$  are a  $(2 \times 2)$  matrix and a vector containing the  $n$ th order term of scattered and incident displacements and stress fields at the heterogeneity boundary. An expansion of coefficients  $\mathbf{T}_n$  and  $\mathbf{b}_n$  can be found in Ref. 7.

Solving Eq. (5) for each order  $n$  (until a maximum truncature order  $N$ ), permits to determine coefficients  $A_n$  and  $B_n$  and, from Eq. (3), the stationary displacement field into the heterogeneity and the surrounding medium. One obtains the displacement spectrum by calculating the displacement into the spherical heterogeneity for different frequencies of the incident torsional wave. In the case of a soft spherical heterogeneity embedded into a harder homogeneous medium, the displacement spectrum exhibits resonance frequencies corresponding to resonance eigenmodes. For qualitative description, an example of simulated eigenmodes of a spherical soft heterogeneity with respect to the surrounding material is presented in Figure 2. In this example, the model served to identify eigenfrequencies (140 Hz and 184 Hz) of the first two eigenmodes of a 7.5 mm radius sphere having a complex

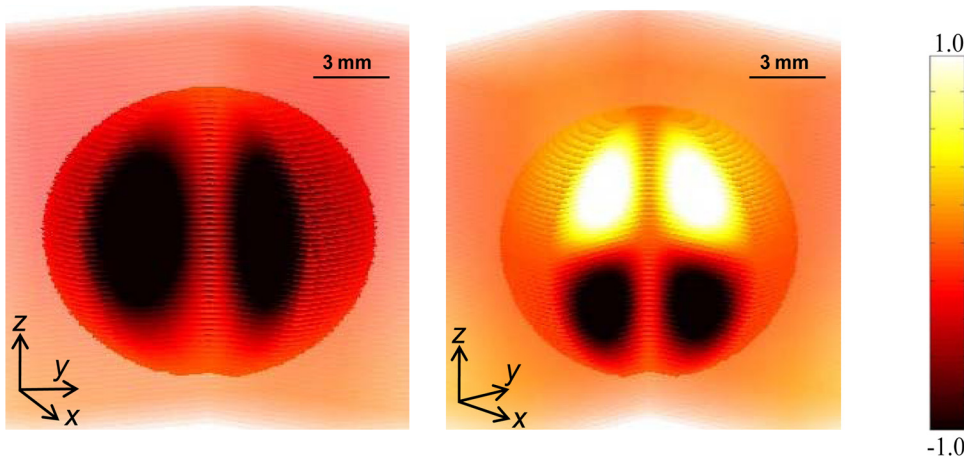


FIG. 2. Qualitative 3D internal views of the first (left) and second (right) simulated eigenmodes (normalized displacements) of a spherical heterogeneity diffracting torsional shear waves.

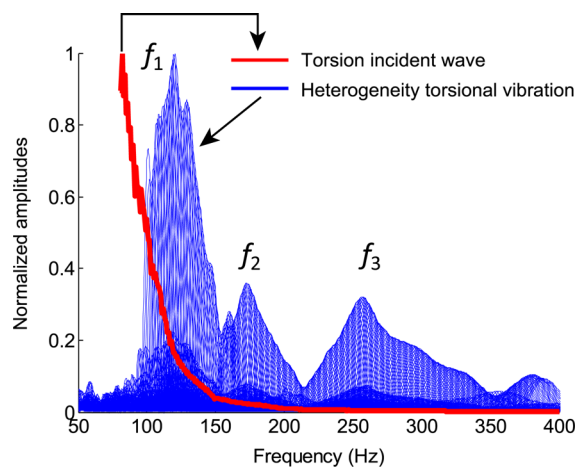


FIG. 3. Experimental resonance spectrum of a spherical 8 mm radius heterogeneity at position  $M$  (+0.5 mm, +3.0 mm, -4.5 mm). Three eigenfrequencies clearly appear:  $f_1 = 120$  Hz,  $f_2 = 172$  Hz, and  $f_3 = 256$  Hz. The shear viscoelastic modulus of the inclusion was  $2700 + 0.5 i\omega$  Pa, whereas that of the surrounding agar-gelatin gel was  $17000 + 0.7 i\omega$  Pa. The measured normalized acceleration spectrum of the spherical cap (correlated to the excitation amplitude) is also represented.

shear modulus of  $2700 + 0.054 i\omega$  Pa, embedded into a homogeneous linear viscoelastic medium presenting a complex shear modulus of  $17600 + 0.7 i\omega$  Pa. One can observe that the first eigenmode induces an in-phase rotation of the spherical inclusion around the symmetry axis of the torsional incident wave, while the second eigenmode produces two hemispheres rotating in phase opposition. In both cases, the heterogeneity appears clearly from its background medium suggesting the potential of SWIRE to segment spherical masses. Both eigenfrequencies and resonance spectra depend on the heterogeneity viscoelastic and geometrical properties. Indeed, the more rigid is the sphere inclusion, the higher are its eigenfrequencies. In the same way, the viscosity affects spectra by reducing displacement amplitudes and the magnitude contrast between eigenfrequencies. It is also noticeable that eigenfrequencies are inversely proportional to the heterogeneity dimension (i.e., its radius).

Experiments were performed on agar-gelatin phantoms and an *in vivo* breast fibroadenoma to assess the feasibility of shear wave resonance induction of spherical heterogeneities. The imaging system was coupled to a vibrating spherical cap

to generate and focus torsional shear waves into the region of interest. Protocol details are given in Ref. 7.

Figure 3 presents the superposition of normalized displacement spectra (normalization with respect to the maximum amplitude spectrum) corresponding to each harmonic torsional wave into a 8.0 mm radius spherical *in vitro* inclusion embedded within a harder medium. The measurement point  $M$  was located into the heterogeneity at  $x = +0.5$  mm,  $y = +3.0$  mm, and  $z = -4.5$  mm in the Cartesian system of coordinates. Three resonance frequencies, i.e., eigenfrequencies, are observed:  $f_1 = 120$  Hz,  $f_2 = 172$  Hz, and  $f_3 = 256$  Hz, each of them corresponding to a torsional eigenmode. Figure 3 also presents the normalized spectral amplitude of the vibrational cap (correlated to the wave amplitude) measured by an accelerometer. The excitation did not exhibit characteristic eigenfrequencies of the heterogeneity.

Eigenmodes of that phantom were experimentally imaged. Figure 4 shows stationary displacement fields corresponding to the first, second, and third eigenmodes. For the two first eigenmodes, displacements into the spherical heterogeneity are greatly enhanced compared with the torsional field in the external medium. Another observation concerns the confinement of the resonant torsional fields into the heterogeneity permitting a clear delimitation of this latter from its background. The third eigenmode in Figure 4(c) shows a less clear definition of the heterogeneity boundary. This is due to the displacement contrast between the inclusion and its environment that is smaller than contrasts observed for the first two eigenmodes.

By using the simulation model, theoretical eigenfrequencies corresponding to the abovementioned experimentation were calculated by using mean values of measured geometrical and mechanical properties of media 1 and 2. Simulated eigenfrequencies were  $f_1 = 127$  Hz,  $f_2 = 175$  Hz, and  $f_3 = 230$  Hz. Biases between theoretical and experimental eigenfrequencies are due to variability of viscoelastic properties of material phantoms (as experienced by Hall *et al.*<sup>8</sup>) and, because of finite dimensions of the medium, to possible wave reflections on phantom boundaries. However, since the maximum bias does not exceed 12%, one can conclude on the good agreement between experimental and theoretical eigenfrequencies.

Figure 5 shows experimental and simulated two-dimensional images of the first two eigenmodes following a plane parallel to  $(oyz)$  for the first mode and  $(oyx)$  for the

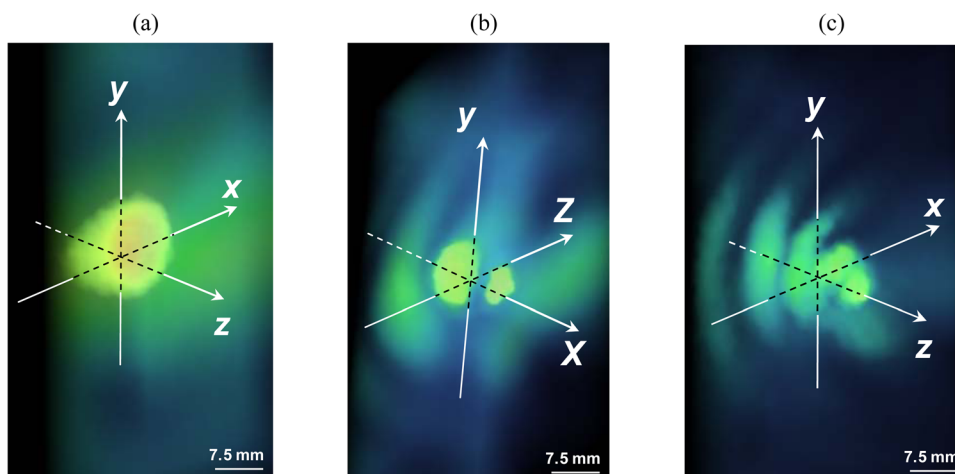


FIG. 4. Experimentally imaged torsional eigenmodes of the spherical inclusion. Displacement amplitude fields at the first eigenfrequency of 120 Hz (a), second eigenfrequency of 172 Hz (b), and third eigenfrequency of 256 Hz (c). A transparency mask was applied to eigenmode images to facilitate the visualization of the internal mechanical response of the spherical heterogeneity.

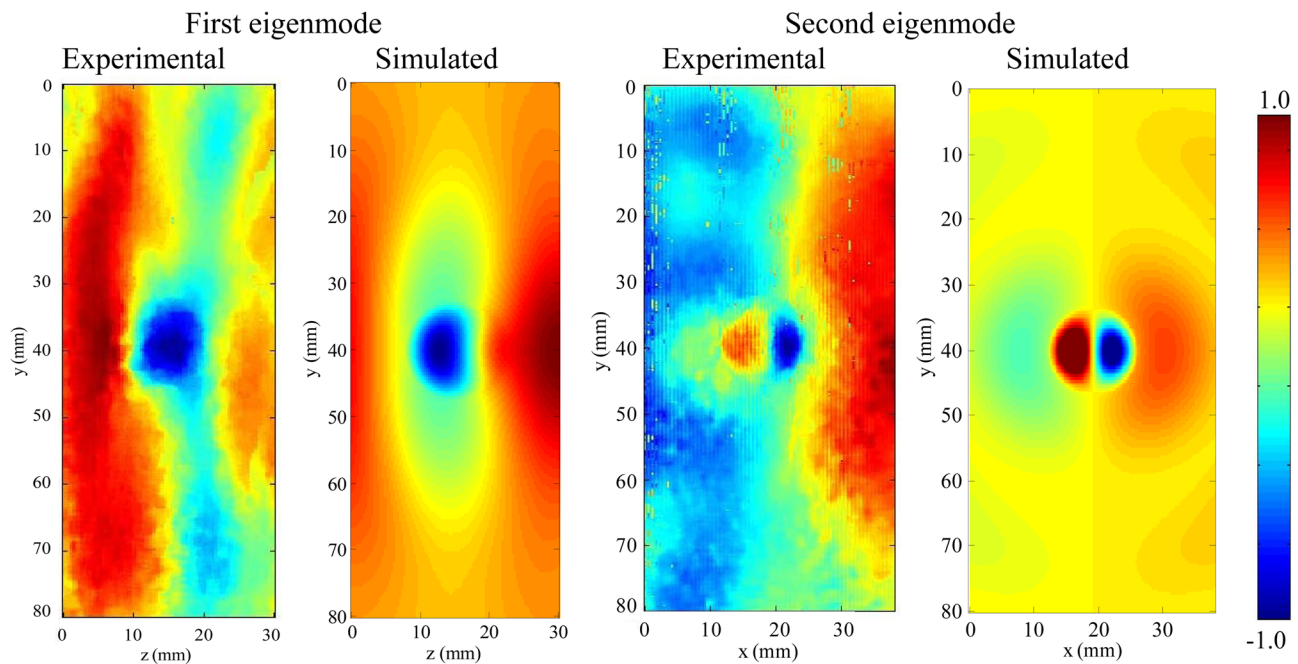


FIG. 5. Experimentally acquired and simulated two-dimensional images of the first two eigenmodes (normalized displacements) of the spherical heterogeneity. Note that one cannot observe the rotation axis as in eigenmode simulated images of Figure 2. This is due to the relatively long wavelength of torsional waves at resonance and to the low resolution of displacement maps. The heterogeneity geometrical imperfections can also make difficult the identification of the torsional axis. In practice and in the context of elastography imaging, this does not limit the validity of the proposed method.

second one. For the first eigenmode, the whole sphere, and the displayed cross-section, vibrates in phase. The second eigenmode is characterized by a phase opposition between two hemispheres. For both eigenmodes, displacement concentration into the heterogeneity allows its clear visual segmentation from the background material. This property is important for future developments in the context of breast imaging and diagnosis. Indeed, a better detectability may allow identify suspected lesions at an earlier stage of development.

Figure 6(a) shows an *in vivo* B-mode image of the scanned 11-mm by 5-mm fibroadenoma at a depth of 30 mm. Panel (b) presents the superimposed stationary displacement map at the first resonance frequency of 80 Hz obtained after a scan of the breast using a set of transient torsional shear waves (having large bandwidths). Clear and confined enhancements of the torsional displacement amplitude are observed into the fibroadenoma.

In this study, shear wave induced resonance elastography was proposed to image spherically shaped mechanical heterogeneities. SWIRE enhances the mechanical dynamical response of the heterogeneity, permits its direct segmentation from resonant displacement images, and is strongly related to the viscoelasticity of the mass. We used focused torsional shear waves to excite resonances. Both experimental resonance frequencies and eigenmodes were in good agreement with the implemented theoretical model. Despite simplified assumptions we made to formulate and to solve the idealized diffraction problem (homogeneous and isotropic media, perfect spherical shape of the heterogeneity), this analytical model had the advantage to facilitate the physical understanding of the resonance induction phenomenon and the interpretation of experimental observations. An important condition to optimally induce resonances of spherically shaped heterogeneities is the use of non-convertible shear

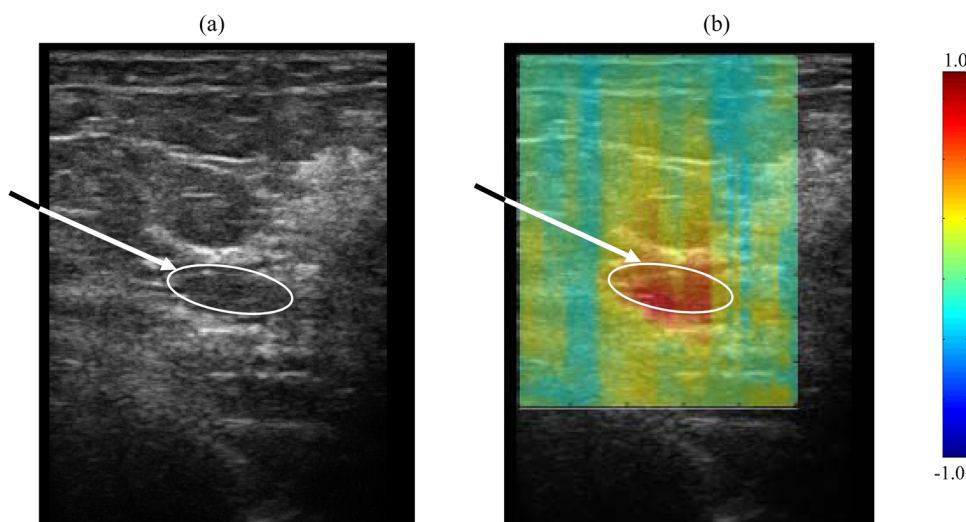


FIG. 6. (a) Ultrasound B-mode image of an 11-mm by 5-mm fibroadenoma (white ellipse) situated deep in the left breast of a 44-year-old woman. (b) Superposition of the ultrasound B-mode image and the normalized stationary displacement map corresponding to an eigenfrequency of 80 Hz.

waves. This condition was satisfied by the use of torsional shear waves that interact experimentally with spheres with minimum mode conversions.

The SWIRE technique has potential for detection and mechanical characterization of breast tumors for diagnosis and therapy monitoring purposes. A preliminary *in vivo* experiment performed using an external excitation set-up presented in Ref. 7 to induce resonance of a fibroadenoma was presented to demonstrate feasibility. Due to the ellipsoidal shape of the scanned fibroadenoma, it was not possible to compare experimental results with the theoretical model since this later is dedicated to spherical heterogeneities. A generalization of the theoretical modeling to consider more complex structures is suitable. In the DE context, this would allow characterizing the viscoelasticity of resonant heterogeneities of arbitrary shapes using an inverse problem approach. The reader is referred to Ref. 7 for details on potential clinical implementations of SWIRE.

This research was jointly supported by the Natural Sciences and Engineering Research Council of Canada (Grant No. CHRP-365656-09) and the Canadian Institutes of Health Research (Grant No. CPG-95288).

<sup>1</sup>M. Tanter, J. Bercoff, A. Athanasiou, T. Deffieux, J. L. Gennisson, G. Montaldo, M. Muller, A. Tardivon, and M. Fink, *Ultrasound Med. Biol.* **34**, 1373 (2008).

<sup>2</sup>A. Samani, J. Zubovits, and D. Plewes, *Phys. Med. Biol.* **52**, 1565 (2007).

<sup>3</sup>A. Hadj Henni, C. Schmitt, and G. Cloutier, *J. Biomech.* **43**, 1488 (2010).

<sup>4</sup>J. D. Achenbach, *Wave Propagation in Elastic Solids* (North-Holland, Amsterdam, 1973).

<sup>5</sup>F. Schwab, *Geophysics* **30**, 24 (1965).

<sup>6</sup>L. Knopoff, *Geophysics* **24**, 209 (1959).

<sup>7</sup>See supplementary material at <http://dx.doi.org/10.1063/1.3696300> for details on expansion of Eq. (5), experimental set-up, and a discussion on clinical implementations.

<sup>8</sup>T. J. Hall, M. Bilgen, M. F. Insana, and T. A. Krouskop, *IEEE Trans. Ultrason. Ferroelectr. Freq. Control* **44**, 1355 (1997).